Protein J (2015) 34:380–390
DOI 10.1007/s10930-015-9632-z

Recombinant Expression of a Functional *Myo*-Inositol-1-Phosphate Synthase (MIPS) in *Mycobacterium smegmatis*

Xinyi Huang[1] · **Marcy Hernick**[1,2]

Published online: 30 September 2015

Abstract *Myo*-inositol-1-phosphate synthase (MIPS, E.C. 5.5.1.4) catalyzes the first step in inositol production—the conversion of glucose-6-phosphate (Glc-6P) to *myo*-inositol-1-phosphate. While the three dimensional structure of MIPS from *Mycobacterium tuberculosis* has been solved, biochemical studies examining the in vitro activity have not been reported to date. Herein we report the in vitro activity of mycobacterial MIPS expressed in *E. coli* and *Mycobacterium smegmatis*. Recombinant expression in *E. coli* yields a soluble protein capable of binding the NAD^+ cofactor; however, it has no significant activity with the Glc-6P substrate. In contrast, recombinant expression in *M. smegmatis* $mc^2$4517 yields a functionally active protein. Examination of structural data suggests that MtMIPS expressed in *E. coli* adopts a fold that is missing a key helix containing two critical (conserved) Lys side chains, which likely explains the inability of the *E. coli* expressed protein to bind and turnover the Glc-6P substrate. Recombinant expression in *M. smegmatis* may yield a protein that adopts a fold in which this key helix is formed enabling proper positioning of important side chains, thereby allowing for Glc-6P substrate binding and turnover. Detailed mechanistic studies may be feasible following optimization of the recombinant MIPS expression protocol in *M. smegmatis*.

Keywords *Myo*-inositol-1-phosphate synthase (MIPS) · Mycobacteria · Recombinant expression · *Mycobacterium smegmatis* · *Mycobacterium tuberculosis*

Abbreviations

Af	*Archaeoglobus fulgidus*
DTT	Dithiothreitol
Glc-6P	Glucose-6-phosphate
IMAC	Immobilized metal ion affinity chromatography
IMP	Inositol monophosphatase
Ins-1P	*Myo*-inositol-1-phosphate
IPTG	Isopropyl β-D-thiogalactopyranoside
KPG	5-Keto-glucose-6-phosphate
LAM	Lipoarabinomannan
LM	Lipomannan
MESG	2-Amino-6-mercapto-7-methylpurine riboside
MIPS	*Myo*-inositol-1-phosphate synthase
Ms	*Mycobacterium smegmatis*
MSH	Mycothiol
Mt	*Mycobacterium tuberculosis*
NTA	Nitrilotriacetic acid
ORF	Open reading frame
PI	Phosphatidyl-*myo*-inositol
PIMs	Phosphatidyl-*myo*-inositol mannosides
PNP	Purine nucleoside phosphorylase
Sc	*Saccharomyces cerevisiae*
TB	Tuberculosis
TCA	Trichloroacetic acid
TCEP	Tris (2-carboxyethyl) phosphine
TEV	Tobacco etch virus

Electronic supplementary material The online version of this article (doi:10.1007/s10930-015-9632-z) contains supplementary material, which is available to authorized users.

✉ Marcy Hernick
mhernick@acp.edu

[1] Department of Biochemistry, Virginia Tech, Blacksburg, VA 24061, USA

[2] Department of Pharmaceutical Sciences, Appalachian College of Pharmacy, Oakwood, VA 24631, USA

1 Introduction

Mycobacterium species, including the causative agents of tuberculosis (TB) and leprosy, possess enzymes that metabolize *myo*-inositol derivatives rarely found in bacteria [1–3]. In these organisms, *myo*-inositol is utilized as a precursor for the production of phosphatidyl-*myo*-inositol (PI) and mycothiol (MSH), which carry out important cellular functions [2, 3]. PI is further elaborated to phosphatidyl-*myo*-inositol mannosides (PIMs), lipomannan (LM), and lipoarabinomannan (LAM), which are unique glycolipids found in the mycobacterial cell envelope [2, 3]. PIMs and LAM play important roles in the interference of phagosome maturation during TB infection, resulting in adaptation to the host and a decreased inflammatory immune response [4]. MSH is the primary reducing agent in mycobacterial species, and is also involved in drug detoxification and TB persistence [5, 6]. Consequently, enzymes involved in the metabolism of inositol derivatives are considered attractive drug targets for the treatment of TB.

Inositol found in mycobacteria can be obtained from the environment using an active inositol-transport system or synthesized de novo through a conserved pathway involving two enzymatic reactions [2, 3, 7, 8]. *Myo*-inositol-1-phosphate synthase (MIPS) converts glucose-6-phosphate (Glc-6P) to *myo*-inositol-1-phosphate (Ins-1P), which is then further hydrolyzed by inositol monophosphatase (IMP) to generate *myo*-inositol (Fig. 1). The *Mycobacterium tuberculosis* MIPS enzyme (MtMIPS) is encoded for by the *Rv0046c (ino1)* gene [9, 10]. MIPS enzymes are clustered into two distinct phylogenetic branches, one containing the smaller bacterial and archaeal enzymes (~40 kDa) and another containing the larger (~60 kDa) eukaryotic orthologs [11]. Sequence analyses suggest that the *ino1* gene encoding for mycobacterial MIPS was recruited from archaea [12]. Inhibition of mRNA expression of MtMIPS results in enhanced susceptibility to antibiotics demonstrating the importance of MtMIPS function [13]. Additionally, a *M. tuberculosis* mutant lacking a functional *ino1* can only be isolated when the growth medium is supplemented with exogenous inositol (77 mM), indicating that MtMIPS is an essential enzyme for inositol synthesis [8]. Rapid killing of *ino1* mutants may result from reduced levels of MSH that render the bacteria susceptible to oxidative stress in macrophages [8]. The virulence of *M. tuberculosis ino1* mutants is severely attenuated such that they are incapable of causing disease in a SCID mouse model [14, 15].

The crystal structure of MIPS from *M. tuberculosis* containing a bound NAD^+ and Zn^{2+} has been solved (Table 1) [16]. The MtMIPS monomer (Fig. 2a; PDB 1GR0) contains a Rossmann fold domain that is responsible for binding NAD^+, as well as a tetramerization domain comprised primarily of β-sheets. The assembled tetramer is shown in Fig. 2b. The presence of a bound a zinc ion in the active site lead to questions regarding whether the mycobacterial enzyme functions through a type III aldolase mechanism requiring monovalent (i.e., ammonium ions) like eukaryotic MIPS enzymes or a type II aldolase mechanism that involves a divalent cation (e.g., zinc or manganese) as observed for archaeal MIPS enzymes [2, 17–21]. Both mechanisms require (catalytic) NAD^+. Initially, a hydride is transferred from Glc-6-P to NAD^+ to generate the keto-Glc-6P (KPG) intermediate and NADH, and in a later step the hydride is transferred back from NADH to an inosose intermediate to generate Ins-1P and NAD^+ [22, 23]. In order address these mechanistic questions, we sought to recombinantly express and purify sufficient quantities of MtMIPS that would allow for detailed biochemical studies of this important enzyme.

Herein we report on the cloning and recombinant expression of MtMIPS and MsMIPS in *E. coli* and *M. smegmatis*. We constructed the mycobacterial expression vector pHALOsmg (Fig. 3) that is derived from the *E. coli-Mycobacterium* shuttle plasmid pYUB1049 [24] and Flexi® vector pFN18K to allow for recombinant expression in *Mycobacterium smegmatis* mc^24517. Recombinant

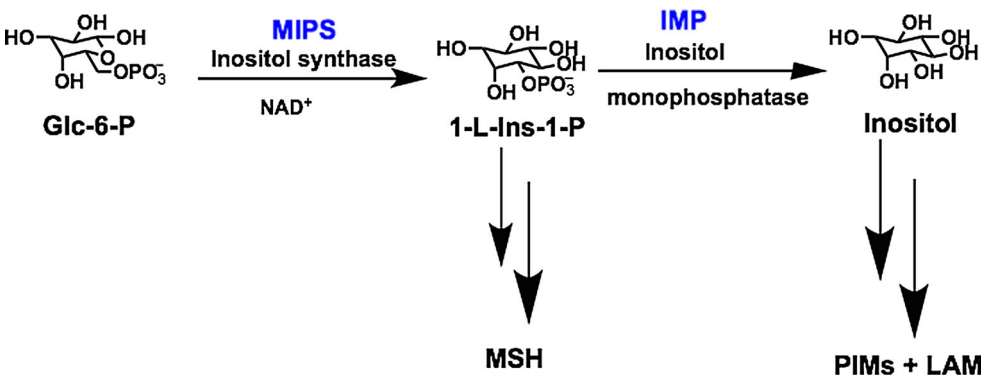

Fig. 1 Inositol biosynthetic and metabolic pathways

Table 1 MIPS crystal structures referenced in these studies

PDB ID	Resolution	Organism	Ligand(s)	Ref.
1GR0	1.95 Å	*Mycobacterium tuberculosis*	NAD^+, Zn^{2+}	[16]
1P1H	1.95 Å	*Saccharomyces cerevisiae*	NAD^+	[48]
1P1J	1.70 Å	*Saccharomyces cerevisiae*	NADH, GOL, PO4	[48]
1U1I	1.90 Å	*Archaeoglobus fulgidus*	NAD^+, K^+, PO4	[20]
3QVT	2.00 Å	*Archaeoglobus fulgidus*	NADH, GOL, KPG, Na^+, PO4, PG4	[47]

GOL glycerol, *KPG* 5-keto-glucose-6-phosphate

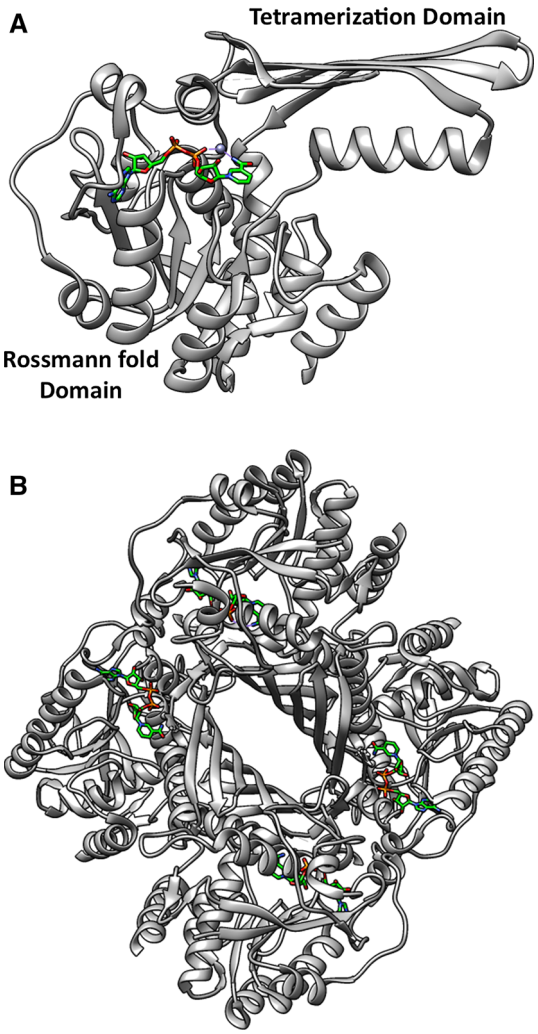

Fig. 2 Crystal structure of *M. tuberculosis* MIPS (PDB 1GR0) containing bound NAD^+ and Zn^{2+}. **a** Monomer; **b** Assembled tetramer

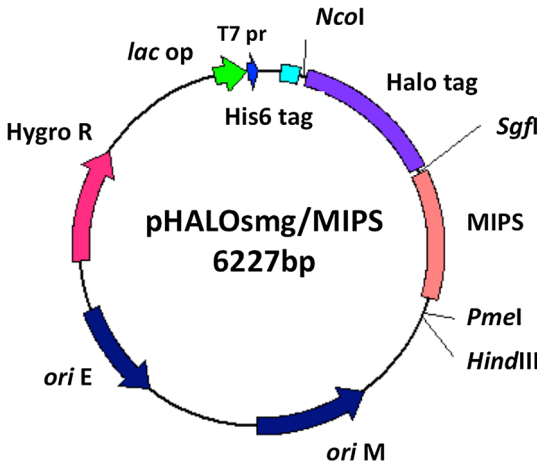

Fig. 3 Arrangement of genetic elements in the pHALOsmg/MIPS expression vector

proteins produced in this study are linked to the N-terminal affinity tags (i.e., His_8-tag, Halo-tag, and His_6-Halo-tag) via a TEV-protease site, which allows for rapid purification and removal of the tag following purification. Recombinant expression of mycobacterial MIPS in *E. coli* yields high quantities of soluble purified protein with no detectable MIPS activity using the Glc-6P substrate. In contrast, recombinant expression of mycobacterial MIPS in *M. smegmatis* yields lower quantities of soluble purified protein with measurable MIPS activity using the Glc-6P substrate. Available structural data suggest that the lack of activity observed for the *E. coli* expressed protein may be attributed to incorrect folding of the protein as a helix containing two critical (conserved) lysine residues is not observed in the MtMIPS crystal structure. Results from these experiments suggest that detailed mechanistic studies on MtMIPS may be feasible following optimization of the recombinant expression protocol in *M. smegmatis*.

2 Materials and Methods

2.1 Materials

All solutions were prepared using milliQ water. *M. smegmatis* and *Mycobacterium bovis* BCG genomic DNA were purchased from ATCC. Primers were purchased from Integrated DNA Technologies. Restriction enzymes were purchased from Promega and New England Biolabs. DNA sequencing was performed at the Virginia Bioinformatics Institute DNA Sequencing Facility (Virginia Tech).

Plasmids and PCR products were purified using the Wizard Plus SV Minipreps DNA Purification System and Wizard SV Gel and PCR Clean-up kits (Promega), respectively. All chemicals were purchased from Gold Biotechnology, Sigma-Aldrich, and ThermoFisher Scientific except where noted. IMP from bovine brain was purchased from Sigma. D-*myo*-inositol-3-phosphate sodium salt (equivalent to L-*myo*-inositol-1-phosphate) was purchased from Cayman Chemical. 2-amino-6-mercapto-7-methylpurine riboside (MESG), purine nucleoside phosphorylase (PNP) and phosphate standard for the IMP-coupled assay were purchased from Invitrogen (EnzChek Phosphate Assay Kit). Phosphate standard (HPLC grade, 1000 mg/L) for the periodate assay was purchased from Dionex. Absorbance and fluorescence measurements were made using a SpectraMax 5M^e plate reader. All protein assays were carried out in 96-well plates (UV or fluorescence, ½ area, Corning).

2.2 Cloning

The open reading frame (ORF) encoding MIPS from *M. bovis* BCG (*Rv0046c*) and *M. smegmatis* (*MSMEG_6904*) were cloned from genomic DNA into the *E. coli* expression vectors pVP55A (N-terminal His_8-TEV-tag) [25] and pFN18K (N-terminal Halo-TEV-tag, Promega) [26] using Flexi® technology (Promega) to generate pVP55A/MIPS and pFN18K/MIPS as previously described for MshB (see Supplemental Material) [27]. The purified recombinant *ino1* proteins from *M. bovis* BCG and *M. smegmatis* are termed MtMIPS and MsMIPS, respectively. To transfer the cloned genes into a mycobacterial expression system, the primer pair of Halo_1 (CATGCCATGGCAGAAATCGG TACTGGCTTTCCAT) and Halo_2 (CGATAAGCTTG GTACCGAGCCCGAATTCGTTTAAAC) was used to amplify the ORF of Halo-TEV-MIPS from the pFN18K/MIPS vector. The resulting PCR fragment contains *NcoI* and *HindIII* restriction sites at 5′ and 3′ ends, respectively. The *NcoI/HindIII* digested PCR product was cloned to the *E. coli–Mycobacterium* shuttle vector pYUB1049 (provided by Dr. Jacobs, Albert Einstein College of Medicine) [24] to produce pHALOsmg/MIPS (Fig. 3). The resulting expression vector pHALOsmg contains a replication origin of *E. coli* (*ori* E) and *M. smegmatis* (*ori* M), a copy of the hygromycin resistance gene, the inducible *lac* operon, and the T7 promoter (from pYUB1049), and yields a recombinant protein with a N-terminal His_6-HaloTag that can be removed following cleavage with TEV protease (from pFN18K). Since the *PmeI* and *SgfI* restriction sites were cloned to the pYUB1049 plasmid along with the MsMIPS ORF, the MIPS ORF from *M. bovis* BCG was cloned to pHALOsmg using Flexi® technology.

2.3 Recombinant Expression of MIPS

Recombinant expression and purification of the target proteins was carried out as previously reported for MshB (see Supplemental Material) [27, 28]. For recombinant expression in *M. smegmatis*, electrocompetent *M. smegmatis* $mc^2$4517 (provided by Dr. Jacobs, Albert Einstein College of Medicine) cells were transformed with pHALOsmg/MIPS expression vectors by electroporation [29]. Briefly, electrocompetent *M. smegmatis* $mc^2$4517 cells (40 µL) were added to a 2 cm cuvette containing pHALOsmg/MIPS (1 µL) and 10 % glycerol (260 µL). Electroporation using a Gene Pulser (BioRad) electroporation system was performed using the following parameters of: $R = 1000\ \Omega$, $Q = 25$ µF, and $V = 2.5$ kV. After one pulse, cells were transferred into 1 mL of 7H9/ADC/Tween and allowed to recover at 37 °C for 3 h. Positive transformants were selected from 7H10 agar plates supplemented with kanamycin (50 µg/mL) and hygromycin (50 µg/mL) after 3–4 days of growth at 37 °C. A single colony of the transformed cells was used to inoculate 5–10 mL 7H9/ADC/Tween and the cells were grown with shaking (250 rpm) at 37 °C for 36 h. For small-scale feasibility studies, the starter culture (4 mL) was used to inoculate LBT (100 mL). The cells were grown with shaking (250 rpm) until an OD_{600} of ~0.6 was reached. Protein expression was induced by the addition of 0.6 mM IPTG, and the cells were continued to be shaken at 37 °C for an additional 3 days. For large-scale expression, the starter culture (1 mL) was added to 1 L ZYP-5052 auto-induction medium and cells were allowed to grow for an additional 3 days at 37 °C with shaking (250 rpm) [24, 29, 30]. Cells were harvested by centrifugation and resuspended in either Buffer A (30 mM HEPES, 150 mM NaCl, 0.5 mM imidazole, pH 7.5) for IMAC purification (large-scale expression) or in Buffer B (30 mM HEPES, 150 mM NaCl, and 1 mM TCEP, pH 7.5) for HaloLink™ purification (small-scale preparation). Resuspended cells were lysed using an Emulsiflex-C3 high-pressure homogenizer (Avestin) and the resulting cell lysates were clarified by centrifugation (18,000 rpm, 4 °C). Clarified cell lysates were loaded onto pre-equilibrated affinity columns and purified as previously described for MshB (see Supplemental Materials) [27].

2.4 Gel Filtration

The solution molecular weight of purified MIPS proteins were determined using size exclusion chromatography with a Superdex 200 10/300 GL column pre-equilibrated with 50 mM sodium phosphate and 150 mM NaCl (pH 7.5) (see Supplemental Materials) [31]. Elution volumes were used to calculate K_{av} values [$K_{av} = (V_e - V_0)/(V_t - V_0)$, where

V_0 is the void volume of the column, V_t is the total volume of the column, and V_e is the elution volume of the protein]. Standard curves were prepared with the following protein standards (GE Healthcare): aprotinin, 6.5 kDa; ovalbumin, 44 kDa; and conalbumin, 75 kDa.

2.5 MIPS Enzyme Activity

MIPS activity, specifically the conversion of Glc-6P to Ins-1P, was measured using the periodate (stopped-point) and IMP-coupled (continuous) assays as previously described (see Supplemental Materials) [32, 33]. Briefly, the periodate assay is a stopped-point assay that uses $NaIO_4$ to oxidize and chemically release phosphate from the Ins-1P product and not the Glc-6P substrate. Assay mixtures (100 mM Tris–acetate, 2 mM DTT pH 7.5; 20 mM NH_4Cl; 1–18 μM MIPS; 300 μM NAD^+) were pre-incubated at 30 °C, and the reactions were initiated with the addition of Glc-6-P (0–40 mM). Reactions aliquots were quenched at various time points by the addition of 20 % trichloroacetic acid and the phosphate group on Ins-1P was released with the addition of 0.2 M $NaIO_4$. The released phosphate group was detected following reaction with ammonium molybdate/ascorbic acid by monitoring the increase in absorbance at 820 nm. In the IMP-coupled assay, the conversion of Glc-6P to Ins-1P is continuously measured by sensing phosphate formation following enzymatic cleavage of Ins-1P using IMP (Fig. 1). Inorganic phosphate released by IMP was detected following reaction with 2-amino-6-mercapto-7-methylpurine riboside (MESG) and purine nucleoside phosphorylase (PNP), which leads to an increase in absorbance at 360 nm. Assay mixtures (50 mM Tris, 1 mM $MgCl_2$, pH 7.5; containing 20 mM NH_4Cl; 300 μM NAD^+; 0.6 mg IMP; 0.2 mM MESG; 4 U/mL PNP; 0.5–18 μM MIPS) were pre-incubated at 30 °C, and the reactions were initiated with the addition of Glc-6P (0–40 mM). Phosphate production was monitored by measuring the absorbance at 360 nm at various time points, and the rate of phosphate production (μM min^{-1}) was calculated from a phosphate standard curve. Relative rates of phosphate production correspond to rate of phosphate production (μM min^{-1}) per 1 μM MIPS.

The affinity of NAD^+ for MIPS was measured by monitoring the decrease of intrinsic MIPS fluorescence intensity upon NAD^+ binding [17, 19]. In these experiments, NAD^+ (0–1 mM) was added to a solution of MIPS (40 μM) in buffer (100 mM HEPES, 400 μM EDTA, pH 7.5; total volume 100 μL). The fluorescence signal of the enzyme mixture (Excitation wavelength = 280 nm, Emission wavelength = 334 nm) was recorded following incubation at room temperature for 5 min in the dark. The decrease in the intrinsic fluorescence of MIPS upon the addition of NAD^+ was plotted as $\Delta I_{fl} = I_0 - I$ (ΔI_{fl}, decrease in MIPS intrinsic fluorescence; I_0, fluorescence of MIPS before adding NAD^+; I, fluorescence of MIPS after adding NAD^+). The apparent K_D of MIPS for NAD^+ was obtained by fitting a binding isotherm equation to the resulting data (Eq. 1). Binding of NAD^+ to MIPS from *Archaeoglobus fulgidus* and *Arabadopsis thaliana* using this method are included in Supplemental Material (Figure S2).

$$\Delta Fl = \Delta Fl_{\max} * \frac{[NAD^+]_{Total}}{(K_D + [NAD^+]_{Total})} + \Delta Fl_{initial} \quad (1)$$

2.6 Computational Studies

Sequence alignment was carried out using the Align feature in ExPASy [34]. Three-dimensional homology models of MIPS from *M. tuberculosis* and *M. smegmatis* were generated using the Phyre 2 protein fold recognition server [35]. Structural alignment of the generated models with MIPS from *M. tuberculosis* (PDB 1GR0), *A. fulgidus* (PDB 3QVT) and *S. cerevisiae* (PDB 1P1J) were carried out using the MatchMaker program in the UCSF Chimera package [36, 37]. For clarity, following alignment figures were generated for the MIPS model, MtMIPS, AfMIPS, and ScMIPS for each orientation by displaying one protein ribbon at a time with KPG and NADH ligands. All molecular graphics images were created using UCSF Chimera [36, 37].

3 Results

3.1 Recombinant Expression of MIPS in *E. coli* Yields an Inactive Protein

Recombinant MsMIPS and MtMIPS proteins were successfully expressed in *E. coli* and purified using a simple His-tag (yield: ~60 mg/L, Supplementary Material). Purified MIPS proteins were assayed for the ability to convert Glc-6P to Ins-1P using two different methods—a periodate (stopped-point) assay and an IMP-coupled (continuous) assay [32, 33, 38]. Two different assays were used for measuring MIPS activity since each has limitations—the periodate assay is labor intensive, but tolerates additives such as divalent metal ions, while the IMP-coupled assay is much less labor intensive, but is significantly affected by the presence of divalent metal ions [32]. Unfortunately, the purified MsMIPS and MtMIPS enzymes recombinantly expressed in *E. coli* exhibited no detectable activity with either assay even in the presence of various additives (0–50 mM $ZnSO_4$ ($ZnCl_2$, Zn-acetate), 0–50 mM $MnCl_2$, 0–50 mM $CoCl_2$, 0–1 mM EDTA,

0–40 mM NH_4Cl, or 0–20 % glycerol). Additionally, the purified proteins did not have any measurable activity using a NADH production assay [19]. Therefore, we attempted to obtain active MIPS using the following approaches: (1) adding a DEAE column to the purification protocol (Supplemental Material Figure S1) prior to the initial IMAC column to remove potential contaminants or proteases that affect MIPS activity, (2) using phosphate-buffered saline and/or glycerol (10 %) containing buffers during the purification protocol to enhance protein stability, and (3) expressing the protein as a Halo-tagged protein and purifying it on HaloLink^{TM} resin to circumvent possible complications from improperly folded proteins or the presence of metal ions (Ni^{2+}). While (soluble) purified MIPS enzyme was obtained using all of these approaches, none yielded a protein with the ability to convert Glc-6P to Ins-1P.

The observed lack of activity with the recombinant MIPS proteins was unexpected given that the crystal structure of MtMIPS was solved using a His-tagged protein recombinantly expressed in *E. coli* [16]. Since a bound NAD^+ is observed in the MtMIPS structure (Fig. 2), we probed whether the purified MIPS proteins were capable of binding NAD^+ using an assay that monitors the decrease in the intrinsic fluorescence of MIPS upon NAD^+ binding [17]. Following excitation at 280 nm, the fluorescence spectrum of MtMIPS exhibits a maximum emission peak at 334 nm. The intensity of this intrinsic fluorescence, but not the maximum emission, decreases upon the addition of NAD^+ (300 μM) with an apparent K_D^{NAD+} of 36 ± 4 μM (Fig. 4). Subsequent addition of Glc-6P (50 mM) to the MtMIPS/NAD^+ mixture results in a slight increase in the fluorescence intensity. While the apparent K_D value indicates that NAD^+ does bind to the mycobacterial MIPS, it is weaker than the apparent K_D values for NAD^+ binding to MIPS from *A. fulgidus* (1 μM) [19] and *A. thaliana* (~0.2 μM, Supplementary Material).

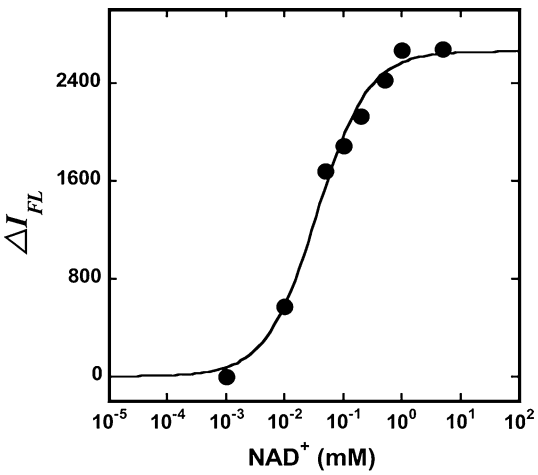

Fig. 4 NAD^+ Binding to MsMIPS. NAD^+ (0–0.1 mM) binding to MsMIPS (40 μM) was determined at pH 7.5 by monitoring the decrease in intrinsic fluorescence (Ex. 280 nm, Em. 334 nm) as described in Sect. 2. The apparent K_D^{NAD+} value was determined to be 36 ± 4 μM using this approach

3.2 Recombinant Expression of MIPS in *M. smegmatis* Yields a Functional Protein

Recombinant expression of *M. tuberculosis* proteins in *E. coli* often results in improperly folded proteins, which can be circumvented by recombinant expression of the proteins using a *M. smegmatis* host [24, 39]. Recombinant expression in *M. smegmatis* offers the following advantages over *E. coli* for the expression of mycobacterial proteins: the presence of mycobacterial chaperones (differ from *E. coli* chaperones) to ensure proper folding, ability to carry out post-translational modification of mycobacterial proteins, and presence of ligands not present in *E. coli* [39]. To probe whether the lack of activity we observed with the recombinant MtMIPS and MsMIPS proteins could be attributed to expression in an *E. coli* host, we recombinantly expressed the MIPS proteins using a *M. smegmatis* expression system. To this end, we constructed the pHALOsmg/MIPS expression vectors (Fig. 3) that yield recombinant proteins with N-terminal His_6-HaloTags that can be removed after purification following cleavage with TEV protease.

Small-scale expression (100 mL) of the proteins in *M. smegmatis* was used to test feasibility of this approach using purification with the HaloLink^{TM} resin (Supplemental Material Figure S5). In this approach, the Halo-tag on the Halo-MIPS constructs forms a covalent bond to the HaloLink^{TM} resin, and the MIPS is "eluted" by cleavage of Halo-MIPS using TEV protease. This approach yields highly purified protein in a single step, likely due to the fact that the tag forms a covalent bond to the resin. The purified MIPS proteins were assayed for the ability to convert Glc-6P to Ins-1P using the periodate (stopped-point) assay [32, 33, 38]. To control for the possibility of the HaloLink resin purifying a contaminant protein from the *M. smegmatis* cell lysate that is capable of phosphate production under the assay conditions used, we also measured phosphate production for MshB deacetylase expressed in *M. smegmatis* and purified using the HaloLink^{TM} resin as a control. The MtMIPS and MsMIPS expressed in *M. smegmatis* show significant activities (~0.1–0.3 μM/min) with 2 mM Glc-6P compared to MIPS expressed from *E. coli* (<0.01 μM/min) using the periodate assay (Fig. 5a). These experiments were done in the presence of zinc (50 μM) since a bound zinc ion is bound to MtMIPS in the crystal structure [16]. No significant activity is observed with the MshB control protein (Fig. 5a, Lane 5) indicating that the

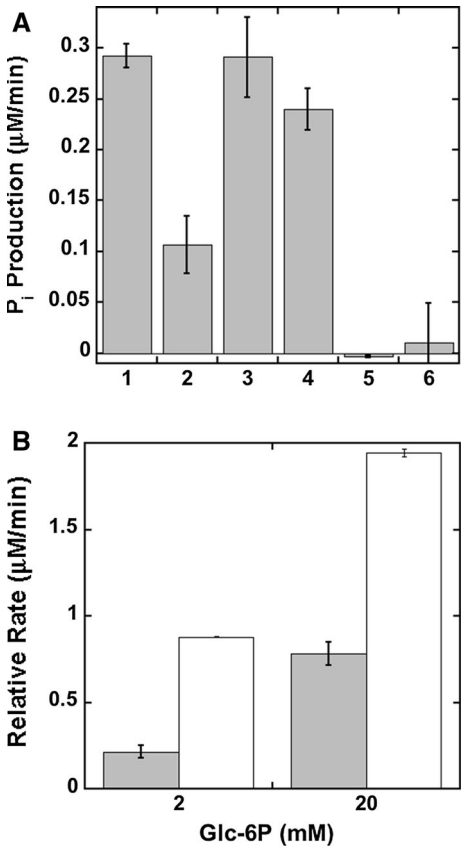

Fig. 5 MIPS activity. **a** Relative activity of mycobacterial MIPS from small-scale expression in *M. smegmatis* using the periodate assay. Rates reflect the phosphate production catalyzed by 1 μM MIPS (in assay buffer containing: 2 mM Glc-6P, 300 μM NAD^+, 20 mM NH_4Cl, 50 μM $ZnSO_4$) as described in Sect. 2. (1) MtMIPS (no NH_4Cl); (2) MtMIPS; (3) MsMIPS (no NH_4Cl), (4) MsMIPS; (5) MshB (control); and (6) MsMIPS (expressed in *E. coli*). **b** Relative activity of mycobacterial MIPS from large-scale expression in *M. smegmatis* using the periodate (*gray bars*) and IMP-coupled (*white bars*) assays. Rates reflect the phosphate production catalyzed by 1 μM MIPS with (300 μM NAD^+, 20 mM NH_4Cl, no $ZnSO_4$) as described in "Supporting Materials"

observed phosphate production can be attributed to the MIPS enzyme. The relative rate of ~0.3 μM/min corresponds to a specific activity of ~1.5×10^{-3} μmol/min/mg for MtMIPS, which is somewhat lower than the specific activities for MIPS from other organisms characterized to date, such as *A. fulgidus* (11.8 μmol/min/mg [17]), *Arabidopsis thaliana* (~0.1 μmol/min/mg [33]), *Saccharomyces cerevisiae* (0.41 μmol/min/mg [40, 41]), and *Synechocystis sp.* (0.02 μmol/min/mg [40]).

In light of these promising results, large-scale expression (1 L) of MtMIPS and MsMIPS in *M. smegmatis* was carried out and the resulting proteins were purified using the His-tag (IMAC). The activity of purified MtMIPS from the large-scale expression with 2 mM Glc-6P using the periodate assay (no zinc) is comparable to the rate observed for the MtMIPS from the small-scale protein expression that was purified using the Halo-tag in the presence of zinc (50 μM, Fig. 5b). The activity is increased at higher Glc-6P concentrations (20 mM) yielding specific activities that are closer to values reported for other MIPS enzymes (*S. cerevisiae* and *Synechocystis sp.*). MIPS activity was also measured using the IMP-coupled assay (Fig. 5b). The relative activities using the IMP-coupled assay are ~twofold higher than the activities measured using the periodate assay.

3.3 Solution Molecular Weight

The majority of MIPS proteins from different species are known to be tetramers in solution, including *A. fulgidus* and *S. cerevisiae*, [16, 17, 20, 21, 42–44] while MIPS from *Neurospora crassa* is a hexamer [18] and MIPS from various plant sources [45] and rat testis [46] are trimeric proteins. The solution molecular weight of recombinant MIPS expressed in *E. coli* and *M. smegmatis* were determined using size exclusion chromatography (Supplemental Materials Figure S3) [31]. Results from these experiments indicate that the MIPS purified from *E. coli* has a solution molecular weight of 140 kDa, or ~3.5 monomers, suggesting that some of the MIPS is present as a trimer in solution. MIPS purified from *M. smegmatis* had two peaks in the elution profile. One peak corresponds to a molecular weight of ~41 kDa, while the second corresponds to a relatively broad peak spanning the range of 248–283 kDa. The protein with the observed molecular weight of ~41 kDa is likely the monomeric Halo-tag protein (34 kDa) [26], and not the MtMIPS monomer, since there are two distinct bands visible on the SDS-PAGE following IMAC purification and the lower band is not observed when the Halo-MIPS protein is purified using the Halo-Link resin that covalently binds to the Halo-tag protein (Supplemental Figure S5). The broad peak spanning the range of 248–283 kDa suggests that the MtMIPS purified following recombinant expression in *M. smegmatis* is a tetramer–hexamer.

3.4 Structural Insights into MIPS Activity

We examined available structures of MIPS enzymes to probe whether they could offer insights into the molecular basis of our findings (select structures summarized in Table 1). Studies examining the catalytic mechanism of archeal/bacterial MIPS (Note: the chemical proposed mechanism for eukaryotic MIPS enzymes is distinct from the archeal/bacterial enzymes [21]) have identified residues (AfMIPS numbering) Asp225, Lys274, Lys278, Lys306, and Lys367 as important for proton transfer reactions in the chemical mechanism [19, 21, 47]. Additional residues that may play roles in catalysis are: Asp332 (metal ligand), Asn

255 (active site clustering/crowding), Leu257 (active site clustering/crowding), and Asp261 (metal ligand) [19, 47]. Sequence alignment of the mycobacterial proteins with AfMIPS and ScMIPS (Supplemental Material Figure S4) indicate that these catalytic residues are conserved in the mycobacterial MIPS proteins with the exception of Leu257 (Gly in MtMIPS and MsMIPS). However, residues 242–267 (Af numbering residues 268–293) are not observed in the MtMIPS structure suggesting that this helix is not formed in the protein fold captured in the crystal structure. In structures of MIPS enzymes from other organisms, this helix (residues 242–267) bridges the Rossmann fold domain and tetramerization domain. The AfMIPS tetramer highlighting the location of this helix is shown in Supplemental Material Figure S5. This finding is important since this helix includes Lys248 and Lys 252 (Af numbering: Lys274 and Lys278), which are critical for substrate binding and catalysis [19, 47]. Therefore, we prepared homology models of MtMIPS and MsMIPS using the Phyre 2 server and the top hits from this analysis are shown in Table 2.

To gain insights into ligand binding, the MtMIPS homology model (c1u1iC, template = AfMIPS) was structurally aligned with AfMIPS (PDB 3QVT), MtMIPS (PDB 1GR0), and ScMIPS (PDB 1P1J). The bound NADH and 5-keto-Glc-6P intermediate (KPG) ligands from the AfMIPS structure are displayed in all figures to highlight the locations of the cofactor and substrate binding sites. There is little difference in the binding orientation of the NADH/NAD^+ in the overlayed structures (Supplemental Material). Figures 6a, c depict the MtMIPS homology model with residues 242–267 (not observed in MtMIPS crystal structure) highlighted in pink. Comparison to the MtMIPS crystal structure (PDB 1GR0) in Fig. 6c, d reveals the importance of residues 242–267 in forming the binding site for the KPG ligand. Figures of AfMIPS and ScMIPS in similar orientations are shown in Supplemental Material.

4 Discussion

Recombinant MIPS expressed *E. coli* is capable of binding NAD^+ with a K_D of 36 ± 4 μM, but cannot turnover the Glc-6P substrate. Although these findings were initially unexpected, they are consistent with previously reported studies. Specifically, structural analysis reveals that a key helix comprised of residues 242–267 is missing in the MtMIPS crystal structure. This finding is important because this helix contains K248 and K252 (equivalent to AfIMPS K274 and K278), which are proposed to be important mechanistically for the proton transfer reactions in the conversion of Glc-6P to Ins-1P [47]. Additionally, mutagenesis studies on these side chains indicate that K274A has weakened/no NAD^+ binding and no ability to produce Ins-1P or NADH, while K278A has weakened NAD^+ (K_D = 70 ± 21 μM) and Glc-6P binding and no ability to produce Ins-1P or NADH [19]. Consequently, one possible explanation for the weak NAD^+ binding and the lack of observed activity with the Glc-6P substrate is that the MIPS proteins expressed in *E. coli*, while soluble, are not folded in a catalytically competent conformation. The finding that the solution molecular weights of the recombinant MIPS proteins expressed in *E. coli* and *M. smegmatis* are different is also consistent with the explanation that variations in protein folding/assembly account for the observed differences in the in vitro activities for proteins expressed in *E. coli* and *M. smegmatis*.

Recombinant MIPS expressed *M. smegmatis* is a functional enzyme that is capable of catalyzing the conversion of Glc-6P to Ins-1P. As discussed above, the observed activity for the protein expressed in *M. smegmatis* is attributed to folding of the enzyme in a catalytically competent conformation. The specific activity reported here for the mycobacterial enzyme is lower than that for the MIPS from *A. fulgidus*, but comparable to MIPS from other organisms (*S. cerevisiae* and *Synechocystis sp.*). This

Table 2 Homology model predictions using Phyre 2

Enzyme	Hit	Confidence (%)	Identity (%)	Coverage (%)	Template information
Mt MIPS	c1gr0A	100	100	96	*M. tuberculosis* MIPS
	c3cinA	100	29	94	*T. maritima* MIPS related protein
	c1u1iC	100	20	95	*A. fulgidus* MIPS
	c1vkoA	100	18	95	*C. elegans* MIPS
	c1p1hD	100	21	95	*S. cerevisiae* MIPS
	d1p1ja1	100	22	95	*S. cerevisiae* MIPS
Ms MIPS	c1gr0A	100	91	98	*M. tuberculosis* MIPS
	c3cinA	100	29	97	*T. maritima* MIPS related protein
	c1vkoA	100	20	98	*C. elegans* MIPS
	c1u1iC	100	20	97	*A. fulgidus* MIPS
	c1p1hD	100	24	98	*S. cerevisiae* MIPS
	d1p1ja1	100	25	98	*S. cerevisiae* MIPS

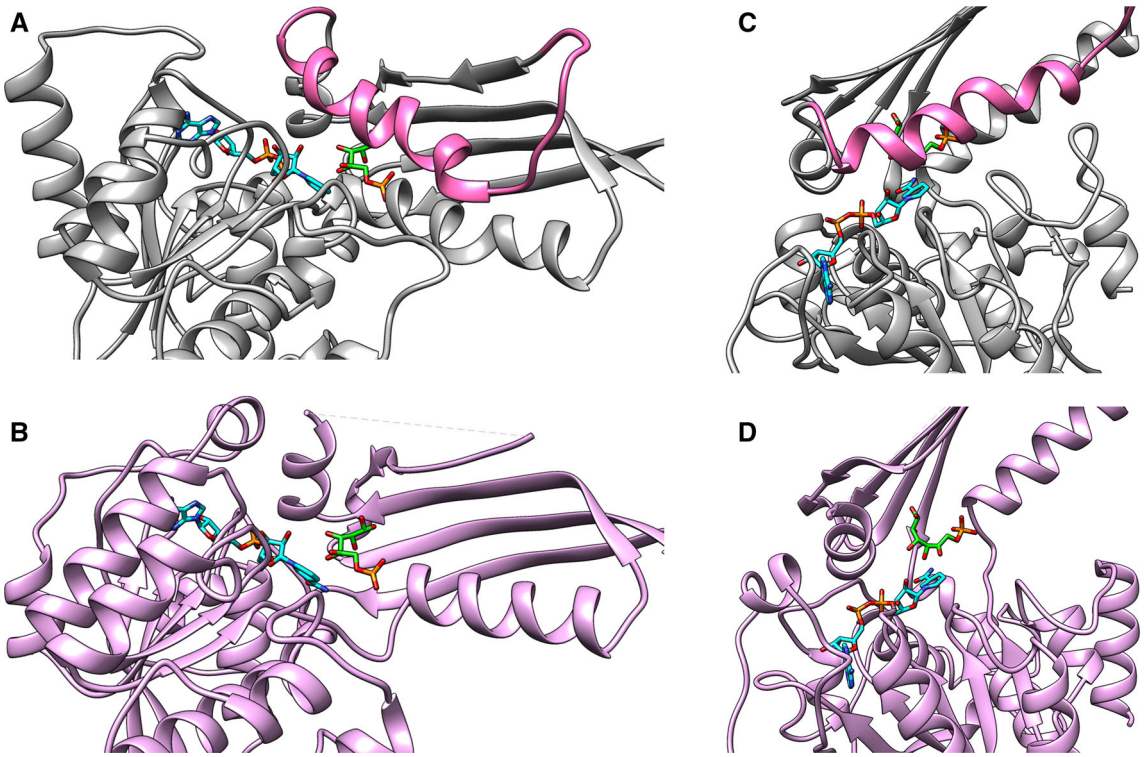

Fig. 6 MIPS with bound KPG (*green*) and NADH (*cyan*) from PDB 3QVT. **a** MtMIPS model in orientation 1 with helix containing residues 242–267 highlighted in *pink*. **b** MtMIPS (PDB 1GR0) in orientation 1. **c** MtMIPS model in orientation 2 with helix containing residues 242–267 highlighted in *pink* **d** MtMIPS (PDB 1GR0) in orientation 2 (Color figure online)

result is also consistent with previous studies. The catalytically important Leu257 (Af numbering) is a glycine in Mt and MsMIPS (Supplemental Materials). The L257A mutation results in a loss of Glc-6P binding, weakened NAD^+ binding ($K_D = 6.5 \pm 3.4$ μM), and an inability to produce Ins-1P/NADH [19]. Consequently, it is not surprising that the mycobacterial enzymes would have reduced activity compared to AfMIPS. Finally, the observed activity of MtMIPS with the IMP-coupled assay is higher than the activity with the periodate assay. Since the activity of AtMIPS is the same using both assays [32], these results may suggest that MtMIPS is stimulated by the presence of the $MgCl_2$ in the IMP-coupled assay buffer or that there are contaminating metal ions from the IMAC column in the purified MIPS that are stimulating enzyme activity.

5 Conclusions

Herein we demonstrate the feasibility of the recombinant expression of MtMIPS and MsMIPS in *M. smegmatis*. Recombinant proteins expressed in *M. smegmatis* are functional, while those expressed in *E. coli* lack measurable activity with the Glc-6P substrate. Structural analysis suggests that MIPS proteins expressed in *E. coli* are not folded in a catalytically competent conformation. Therefore, it is likely that expression in the mycobacterial host enables the protein to fold in a catalytic conformation. Optimization of the MIPS expression and purification protocol in *M. smegmatis* will allow for detailed biochemical studies to probe the catalytic mechanism and molecular recognition properties of this important enzyme.

Acknowledgments The plasmid pYUB1049 and strain *Mycobacterium smegmatis* mc^24517 were kindly provided by Dr. William Jacobs, Albert Einstein College of Medicine.

Compliance with Ethical Standards

Conflicts of interest The authors declare no conflicts of interest.

References

1. Michell RH (2008) Inositol derivatives: evolution and functions. Nat Rev Mol Cell Biol 9:151–161
2. Huang X, Hernick M (2013) In: Rocha H, Cardoso M (eds) Inositol derivatives in *Mycobacterium tuberculosis*: function, biosynthesis and therapeutic implications. Nova Science Publishers, Hauppauge
3. Morita YS, Fukuda T, Sena CB, Yamaryo-Botte Y, McConville MJ, Kinoshita T (2011) Inositol lipid metabolism in

mycobacteria: biosynthesis and regulatory mechanisms. Biochim Biophys Acta 1810:630–641
4. Mishra AK, Driessen NN, Appelmelk BJ, Besra GS (2011) Lipoarabinomannan and related glycoconjugates: structure, biogenesis and role in *Mycobacterium tuberculosis* physiology and host-pathogen interaction. FEMS Microbiol Rev 35:1126–1157
5. Newton GL, Buchmeier N, Fahey RC (2008) Biosynthesis and functions of mycothiol, the unique protective thiol of Actinobacteria. Microbiol Mol Biol Rev 72:471–494
6. Hernick M (2013) Mycothiol, a target for potentiation of rifampin and other antibiotics against *M. tuberculosis*. Expert Rev Anti-Infect Ther 11:49–67
7. Bettaney KE, Sukumar P, Hussain R, Siligardi G, Henderson PJ, Patching SG (2012) A systematic approach to the amplified expression, functional characterization and purification of inositol transporters from *Bacillus subtilis*. Mol Membr Biol 30:3–14
8. Movahedzadeh F, Smith DA, Norman RA, Dinadayala P, Murray-Rust J, Russell DG, Kendall SL, Rison SC, McAlister MS, Bancroft GJ, McDonald NQ, Daffe M, Av-Gay Y, Stoker NG (2004) The *Mycobacterium tuberculosis* ino1 gene is essential for growth and virulence. Mol Microbiol 51:1003–1014
9. Cole ST, Brosch R, Parkhill J, Garnier T, Churcher C, Harris D, Gordon SV, Eiglmeier K, Gas S, Barry CE 3rd, Tekaia F, Badcock K, Basham D, Brown D, Chillingworth T, Connor R, Davies R, Devlin K, Feltwell T, Gentles S, Hamlin N, Holroyd S, Hornsby T, Jagels K, Krogh A, McLean J, Moule S, Murphy L, Oliver K, Osborne J, Quail MA, Rajandream MA, Rogers J, Rutter S, Seeger K, Skelton J, Squares R, Squares S, Sulston JE, Taylor K, Whitehead S, Barrell BG (1998) Deciphering the biology of *Mycobacterium tuberculosis* from the complete genome sequence. Nature 393:537–544
10. Bachhawat N, Mande SC (1999) Identification of the INO1 gene of *Mycobacterium tuberculosis* H37Rv reveals a novel class of inositol-1-phosphate synthase enzyme. J Mol Biol 291:531–536
11. Bachhawat N, Mande SC (2000) Complex evolution of the inositol-1-phosphate synthase gene among archaea and eubacteria. Trends Genet 16:111–113
12. Majumder AL, Chatterjee A, Ghosh Dastidar K, Majee M (2003) Diversification and evolution of L-myo-inositol 1-phosphate synthase. FEBS Lett 553:3–10
13. Li Y, Chen Z, Li X, Zhang H, Huang Q, Zhang Y, Xu S (2007) Inositol-1-phosphate synthetase mRNA as a new target for antisense inhibition of *Mycobacterium tuberculosis*. J Biotechnol 128:726–734
14. Smith D, Hansch H, Bancroft G, Ehlers S (1997) T-cell-independent granuloma formation in response to *Mycobacterium avium*: role of tumour necrosis factor-alpha and interferon-gamma. Immunology 92:413–421
15. Hansch HC, Smith DA, Mielke ME, Hahn H, Bancroft GJ, Ehlers S (1996) Mechanisms of granuloma formation in murine Mycobacterium avium infection: the contribution of CD4+ T cells. Int Immunol 8:1299–1310
16. Norman RA, McAlister MS, Murray-Rust J, Movahedzadeh F, Stoker NG, McDonald NQ (2002) Crystal structure of inositol 1-phosphate synthase from *Mycobacterium tuberculosis*, a key enzyme in phosphatidylinositol synthesis. Structure 10:393–402
17. Chen L, Zhou C, Yang H, Roberts MF (2000) Inositol-1-phosphate synthase from *Archaeoglobus fulgidus* Is a class II aldolase. Biochemistry 39:12415–12423
18. Escamilla JE, Contreras M, Martinez A, Zentella-Pina M (1982) L-myoinositol-1-phosphate synthase from *Neurospora crassa*: purification to homogeneity and partial characterization. Arch Biochem Biophys 218:275–285
19. Neelon K, Wang Y, Stec B, Roberts MF (2005) Probing the mechanism of the *Archaeoglobus fulgidus* inositol-1-phosphate synthase. J Biol Chem 280:11475–11482
20. Stieglitz KA, Yang H, Roberts MF, Stec B (2005) Reaching for mechanistic consensus across life kingdoms: structure and insights into catalysis of the myo-Inositol-1-phosphate synthase (mIPS) from *Archaeoglobus fulgidus*. Biochemistry 44:213–224
21. Geiger JH, Jin X (2006) In: Majumder AL, Biswas BB (eds) The structure and mechanism of myo-inositol-1-phosphate synthase. Springer, US
22. Stieglitz KA, Yang H, Roberts MF, Stec B (2005) Reaching for mechanistic consensus across life kingdoms: structure and insights into catalysis of the myo-inositol-1-phosphate synthase (mIPS) from *Archaeoglobus fulgidus*. Biochemistry 44:213–224
23. Jin X, Geiger JH (2003) Structures of NAD(+)-and NADH-bound 1-l-myo-inositol 1-phosphate synthase. Acta Crystallogr D Biol Crystallogr 59:1154–1164
24. Goldstone RM, Moreland NJ, Bashiri G, Baker EN, Shaun Lott J (2008) A new Gateway vector and expression protocol for fast and efficient recombinant protein expression in *Mycobacterium smegmatis*. Protein Expr Purif 57:81–87
25. Sobrado P, Goren MA, James D, Amundson CK, Fox BG (2008) A Protein structure initiative approach to expression, purification, and in situ delivery of human cytochrome b5 to membrane vesicles. Protein Expr Purif 58:229–241
26. Peterson SN, Kwon K (2012) The HaloTag: improving soluble expression and applications in protein functional analysis. Curr Chem Genomics 6:8–17
27. Huang X, Kocabas E, Hernick M (2011) The activity and cofactor preferences of *N*-acetyl-1-D-myo-inositol-2-amino-2-deoxy-Œ±-D-glucopyranoside deacetylase (MshB) change depending on environmental conditions. J Biol Chem 286:20275–20282
28. Huang X, Hernick M (2011) A fluorescence-based assay for measuring *N*-acetyl-1-D-myo-inosityl-2-amino-2-deoxy-α-D-glucopyranoside deacetylase (MshB) activity. Anal Biochem 414:278–281
29. Bashiri G, Squire CJ, Baker EN, Moreland NJ (2007) Expression, purification and crystallization of native and selenomethionine labeled *Mycobacterium tuberculosis* FGD1 (Rv0407) using a *Mycobacterium smegmatis* expression system. Protein Expr Purif 54:38–44
30. Studier FW (2005) Protein production by auto-induction in high density shaking cultures. Protein Expr Purif 41:207–234
31. Andrews P (1964) Estimation of the molecular weights of proteins by Sephadex gel-filtration. Biochem J 91:222–233
32. Huang X, Hernick M (2011) A limitation of the continuous spectrophotometric assay for the measurement of myo-inositol-1-phosphate synthase activity. Anal Biochem 417:228–232
33. Donahue JL, Alford SR, Torabinejad J, Kerwin RE, Nourbakhsh A, Ray WK, Hernick M, Huang X, Lyons BM, Hein PP, Gillaspy GE (2010) The *Arabidopsis thaliana* myo-inositol 1-phosphate synthase1 gene is required for myo-inositol synthesis and suppression of cell death. Plant Cell 22:888–903
34. Artimo P, Jonnalagedda M, Arnold K, Baratin D, Csardi G, de Castro E, Duvaud S, Flegel V, Fortier A, Gasteiger E, Grosdidier A, Hernandez C, Ioannidis V, Kuznetsov D, Liechti R, Moretti S, Mostaguir K, Redaschi N, Rossier G, Xenarios I, Stockinger H (2012) ExPASy: SIB bioinformatics resource portal. Nucleic Acids Res 40:W597–W603
35. Kelley LA, Mezulis S, Yates CM, Wass MN, Sternberg MJE (2015) The Phyre2 web portal for protein modeling, prediction and analysis. Nat Protoc 10:845–858
36. Meng E, Pettersen E, Couch G, Huang C, Ferrin T (2006) Tools for integrated sequence-structure analysis with UCSF Chimera. BMC Bioinform 7:339
37. Pettersen EF, Goddard TD, Huang CC, Couch GS, Greenblatt DM, Meng EC, Ferrin TE (2004) UCSF Chimera—a visualization system for exploratory research and analysis. J Comput Chem 25:1605–1612

38. Barnett JE (1970) A colorimetric determination of inositol monophosphates as an assay for D-glucose 6-phosphate-1L-myoinositol 1-phosphate cyclase. Biochem J 119:183–186
39. Bashiri G, Baker EN (2015) Production of recombinant proteins in *Mycobacterium smegmatis* for structural and functional studies. Protein Sci 24:1–10
40. Chatterjee A, Majee M, Ghosh S, Majumder A (2004) sll1722, an unassigned open reading frame of Synechocystis PCC 6803, codes for l-myo-inositol 1-phosphate synthase. Planta 218:989–998
41. Donahue TF, Henry SA (1981) myo-Inositol-1-phosphate synthase. Characteristics of the enzyme and identification of its structural gene in yeast. J Biol Chem 256:7077–7085
42. Majumder AL, Chatterjee A, Dastidar KG, Majee M (2003) Diversification and evolution of -myo-inositol 1-phosphate synthase. FEBS Lett 553:3–10
43. Majumder AL, Johnson MD, Henry SA (1997) 1L-myo-inositol-1-phosphate synthase. Biochim Biophys Acta 1348:245–256
44. Ju S, Greenberg ML (2004) 1D-myo-inositol 3-phosphate synthase: conservation, regulation, and putative target of mood stabilizers. Clin Neurosci Res 4:181–187
45. RayChaudhuri A, Hait NC, Dasgupta S, Bhaduri TJ, Deb R, Majumder AL (1997) L-myo-Inositol 1-phosphate synthase from plant sources (characteristics of the chloroplastic and cytosolic enzymes). Plant Physiol 115:727–736
46. Maeda T, Eisenberg F (1980) Purification, structure, and catalytic properties of L-myo-inositol-1-phosphate synthase from rat testis. J Biol Chem 255:8458–8464
47. Neelon K, Roberts MF, Stec B (2011) Crystal structure of a trapped catalytic intermediate suggests that forced atomic proximity drives the catalysis of mIPS. Biophys J 101:2816–2824
48. Jin X, Geiger JH (2003) Structures of NAD+- and NADH-bound 1-l-myo-inositol 1-phosphate synthase. Acta Crystallogr Sect D 59:1154–1164